LETTER

doi:10.1038/nature10561

Observation of the dynamical Casimir effect in a superconducting circuit

C. M. Wilson[1], G. Johansson[1], A. Pourkabirian[1], M. Simoen[1], J. R. Johansson[2], T. Duty[3], F. Nori[2,4] & P. Delsing[1]

One of the most surprising predictions of modern quantum theory is that the vacuum of space is not empty. In fact, quantum theory predicts that it teems with virtual particles flitting in and out of existence. Although initially a curiosity, it was quickly realized that these vacuum fluctuations had measurable consequences—for instance, producing the Lamb shift[1] of atomic spectra and modifying the magnetic moment of the electron[2]. This type of renormalization due to vacuum fluctuations is now central to our understanding of nature. However, these effects provide indirect evidence for the existence of vacuum fluctuations. From early on, it was discussed whether it might be possible to more directly observe the virtual particles that compose the quantum vacuum. Forty years ago, it was suggested[3] that a mirror undergoing relativistic motion could convert virtual photons into directly observable real photons. The phenomenon, later termed the dynamical Casimir effect[4,5], has not been demonstrated previously. Here we observe the dynamical Casimir effect in a superconducting circuit consisting of a coplanar transmission line with a tunable electrical length. The rate of change of the electrical length can be made very fast (a substantial fraction of the speed of light) by modulating the inductance of a superconducting quantum interference device at high frequencies (>10 gigahertz). In addition to observing the creation of real photons, we detect two-mode squeezing in the emitted radiation, which is a signature of the quantum character of the generation process.

That mirrors can be used to measure vacuum fluctuations was first predicted by Casimir[6] in 1948. Casimir predicted that two mirrors, that is, perfectly conducting metal plates, held parallel to each other in vacuum will experience an attractive force. Essentially, the mirrors reduce the density of electromagnetic modes between them. The vacuum radiation pressure between the plates is then less than the pressure outside, generating the force. As this static Casimir effect can then be explained by a mismatch of vacuum modes in space, the dynamical Casimir effect can be seen as arising from a mismatch of vacuum modes in time. As a mirror moves, it changes the spatial mode structure of the vacuum. If the mirror's velocity, v, is slow compared to the speed of light, c, the electromagnetic field can adiabatically adapt to the changes and no excitation occurs. If instead v/c is not negligible, then the field cannot adjust smoothly and can be non-adiabatically excited out of the vacuum.

The static Casimir effect can also be calculated in terms of the electrical response of the mirrors to the electromagnetic field[7]. A similar complementary explanation exists for the dynamical Casimir effect[3]. An ideal mirror represents a boundary condition for the electromagnetic field—in particular, that the electric field is zero at the surface. This boundary condition is enforced by the flow of screening currents in the metal. A mirror moving in a finite electromagnetic field then loses energy, because the screening currents will emit electromagnetic radiation, as in an antenna. Classically, we expect this radiation damping to be zero in a region where the electric field strength is zero. In quantum theory, however, vacuum fluctuations will always generate screening currents. Therefore, even moving in the vacuum can cause a mirror to emit real photons in response to vacuum fluctuations.

If we consider the real experiment of moving a physical mirror near the speed of light, we quickly see that it is not feasible. This fact has led to a number of alternative proposals[8–20], for instance using surface acoustic waves, nanomechanical resonators, or modulation of the electrical properties of a cavity.

Here we investigate one such proposal using a superconducting circuit[16,17]: an open transmission line terminated by a SQUID (superconducting quantum interference device). A SQUID is composed of two Josephson junctions connected in parallel to form a loop. At the frequencies studied here, the SQUID acts as a parametric inductor whose value, L_J, can be tuned by applying a magnetic flux, Φ_{ext}, through the SQUID loop. When placed at the end of a transmission line, this SQUID can then be used to change the line's boundary condition. In previous work[18,21], we showed that this tuning can be done on very short timescales. The changing inductance can be described as a change in the electrical length of the transmission line and, in fact, provides the same time-dependent boundary condition as the idealized moving mirror[22,23]. In the same way as for the mirror, the boundary condition is enforced by screening currents that flow through the SQUID. Unlike the mirror, the maximum effective velocity of the boundary, v_e, defined as the rate of change of the electrical length, can be very large compared to the speed of light in the transmission line, $c_0 \approx 0.4c$, approaching $v_e/c_0 \approx 0.25$ for large modulations of L_J. The photon production rate is therefore predicted to be several orders of magnitude larger than in other systems[17].

Quantum theory allows us to make more detailed predictions than just that photons will be produced. If the boundary is driven sinusoidally at an angular frequency $\omega_d = 2\pi f_d$, then it is predicted[17,24] that photons will be produced in pairs such that their frequencies, ω_+ and ω_-, sum to the drive frequency, that is, we expect $\omega_d = \omega_+ + \omega_-$. This pairwise production implies that the electromagnetic field at these sideband frequencies, symmetric around $\omega_d/2$, should be correlated. In detail, we can predict that the field should exhibit what is known as two-mode squeezing (TMS)[25].

Theoretically, we treat the problem as a scattering problem in the context of quantum network theory[26] (see Supplementary Information). If the boundary is driven with a small amplitude $\delta\ell_e$, we find that the output photon flux density at frequency ω for an input thermal state is

$$n_{out}(\omega) = n_{in}(\omega) + |S(\omega)|^2 n_{in}(\omega_d - \omega) + |S(\omega)|^2 \qquad (1)$$

where $S(\omega) = -i(\delta\ell_e/c_0)\sqrt{\omega(\omega_d-\omega)}A(\omega)A^*(\omega_d-\omega)$, $A(\omega)$ is the spectral amplitude of the transmission line and $A^*(\omega)$ is its complex conjugate. The first two terms on the right-hand side of equation (1), proportional to the thermal occupation number $n_{in}(\omega)$, represent the purely classical effects of reflection and upconversion of the input field to the drive frequency. They are zero at zero temperature. The last term on the right-hand side is due to vacuum fluctuations and is, in fact, the DCE radiation.

[1]Department of Microtechnology and Nanoscience, Chalmers University of Technology, Göteborg 412 96, Sweden. [2]Advanced Science Institute, RIKEN, Wako-shi, Saitama 351-0198, Japan. [3]University of New South Wales, Sydney, New South Wales 2052, Australia. [4]University of Michigan, Ann Arbor, Michigan 48109, USA.

The photon production rate depends on the density of states in the transmission line, which is $|A(\omega)|^2$. For an ideal transmission line, $A(\omega) = 1$ and the DCE radiation measured at a detuning $\delta\omega$ from $\omega_d/2$ becomes $n_{out}^{DCE}(\varepsilon) = (v_e/2c_0)^2(1-\varepsilon^2)$ where $\varepsilon = 2\delta\omega/\omega_d$ is the normalized detuning and $v_e = \delta\ell_e\omega_d$. The integrated photon flux of the DCE radiation is then $\Gamma_{DCE} = (\omega_d/12\pi)(v_e/c_0)^2$, identical to that of an ideal mirror oscillating in one-dimensional space[23]. The relativistic nature of the effect is apparent here, in that the photon flux goes to zero if we allow the speed of light to go to infinity.

We present measurements on two samples, both of which consist of a SQUID connected to an aluminium coplanar waveguide (CPW). Sample 1 has a long (~43 mm) CPW and sample 2 has a short (~0.1 mm) CPW (Fig. 1a, b). The samples are cooled to ≤50 mK in a dilution refrigerator. This corresponds to a thermal photon occupation number of $n_{in} < 0.01$ at 5 GHz, which is the centre of our analysis band. In separate measurements of qubit circuits in the same set-up, we have demonstrated[27] that the radiation temperature of the system is near the cryostat's base temperature. If we consider the last two terms on the right-hand side of equation (1), which are the response of the system to the changing boundary, we can compare this small value $n_{in} = 0.01$ to the vacuum response, which has a coefficient of 1.

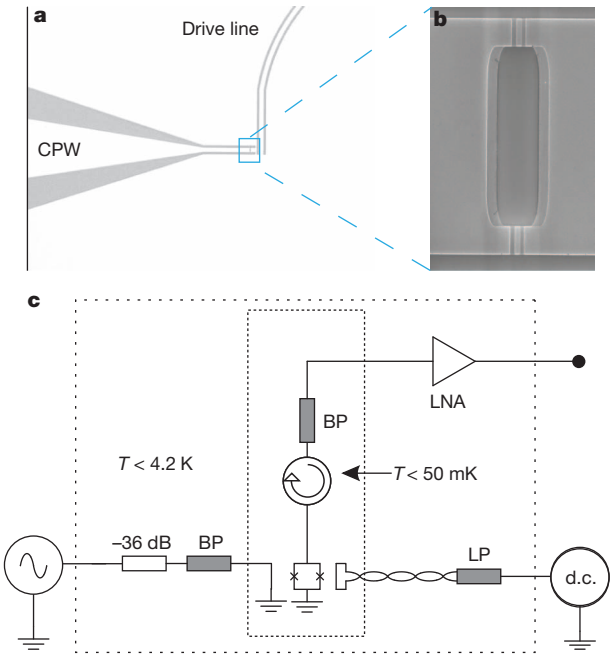

Figure 1 | Experimental overview. **a**, Optical micrograph of sample 2. Light parts are Al, which fills most of the image, while the dark parts are the Si substrate, visible where the Al has been removed to define the transmission lines. The output line is labelled CPW and the drive line enters from the top. Both lines converge near the SQUID (boxed). **b**, A scanning-electron micrograph of the SQUID. The SQUID has a vertical dimension of 13 μm and a normal state resistance of 218 Ω (170 Ω) implying $L_J(0) = 0.23$ nH (0.18 nH) for sample 2 (sample 1). A basic electrical characterization of the SQUID is presented in Supplementary Fig. 1. **c**, A simplified schematic of the measurement set-up. The SQUID is indicated by the box with two crosses, suggestive of the SQUID loop interrupted by Josephson junctions. A small external coil is also used to apply a d.c. flux bias through a lowpass filter (LP). The driving line has 36 dB of cold attenuation, along with an 8.4–12 GHz bandpass filter (BP). The filter ensures that no thermal radiation couples to the transmission line in the frequency region were we expect DCE radiation. (For sample 1, the last 6 dB of attenuation were at base temperature.) The outgoing field of the CPW is coupled through two circulators to a cryogenic low-noise amplifier (LNA) with a system noise temperature of $T_N \approx 6$ K. At room temperature, the signal is further amplified before being captured by two vector microwave digitizers. The dashed boxes delineate portions of the set-up at different temperatures, T, which are labelled.

To study the effects of non-adiabatic perturbations, we drive the flux through the SQUID at microwave frequencies using an inductively coupled CPW line that is short-circuited ~20 μm from the SQUID. We measure the output power from the measurement line as a function of drive power and frequency, $f_d = \omega_d/2\pi$. We start with the analysis frequency tracking the drive at $f_d/2$, where we expect the DCE radiation to be centred. The results are shown in Supplementary Fig. 2. In both samples, we clearly see photon generation for essentially all drive frequencies spanning the 8–12 GHz band set by the filtering of the line. This corresponds to an analysis band of 4–6 GHz.

In the next set of measurements, we fix the drive frequency, but scan the analysis frequency. In this way, we can see over what band photons are produced for fixed drive frequency. In both samples, we clearly see broadband photon production for all the frequencies analysed, including detunings from $f_d/2$ larger than 2 GHz. In Fig. 2a and b, we show results for sample 1. The broadband nature of the photon generation clearly distinguishes the observed phenomenon from that of a parametric amplifier, which has a narrow band defined by a resonator.

We quantify the photon production rate by referencing it to our system noise temperature of $T_N \approx 6$ K, which has been calibrated previously using a shot-noise thermometer[28]. The measured power spectral density is corrected for the transmission variations measured with a network analyser and then divided by the photon energy, $\hbar\omega$, at each analysis frequency to convert to n_{out}. In Fig. 2a and b, we clearly see a corrugated structure in n_{out}, reflecting variations in $A(\omega)$ caused by parasitic reflections in the measurement line at, for example, cable connectors or the input of the amplifier. Overall, we see that n_{out} is clearly symmetric around $f_d/2$, as emphasized in Fig. 2c and d, which strongly indicates that the radiation is produced by the DCE and not by a spurious effect, such as heating.

To make a quantitative comparison to theory, we need to know the drive amplitude, which is difficult to know a priori as the short-circuit termination of the pump line is not matched to the characteristic impedance of the line. We therefore expect the current flowing through the line to be a strong function of frequency. However, we see that n_{out} starts to saturate as a function of drive power above the nominal level of 100 pW (not shown). We now make the reasonable assumption that this saturation is caused by the drive amplitude reaching the level where the modulation of L_J saturates, that is, where the sum of the flux amplitude and d.c. bias flux reaches $0.5\Phi_0$, where $\Phi_0 = h/2e$ is the superconducting flux quantum. For our working point of $\Phi_{ext} = -0.35\Phi_0$, the corresponding flux amplitude is only $0.15\Phi_0$, which we have previously demonstrated is experimentally accessible[21]. For these large modulations, equation (1) is no longer sufficient because higher-order processes become important. However, these processes can be included and n_{out} computed numerically[17]. As shown in Fig. 2e, we find that the calculated n_{out} matches the measured value if we assume modest values of $|A(\omega_+)A(\omega_-)| \approx 2$–4. This corresponds to a voltage standing wave ratio (VSWR) in our measurement line of less than 2, which is reasonable. We note that at these large drives, n_{out} deviates from its linear dependence on drive power, which is proportional to $(v_e/c_0)^2$. However, we see in Fig. 2e that the full theory[17] captures this deviation well. We also comment that, in making the calculation, we have made a model of the electromagnetic environment, encapsulated in $A(\omega)$, to high frequencies. There is a great deal of uncertainty in doing this. However, with a basic physical model, we see that we are able to reproduce both the magnitude and drive dependence of n_{out}.

Theory[17] also predicts that the output should exhibit voltage–voltage correlations, known as TMS. Experimentally, we measure the four quadrature voltages of the upper and lower sidebands, corresponding

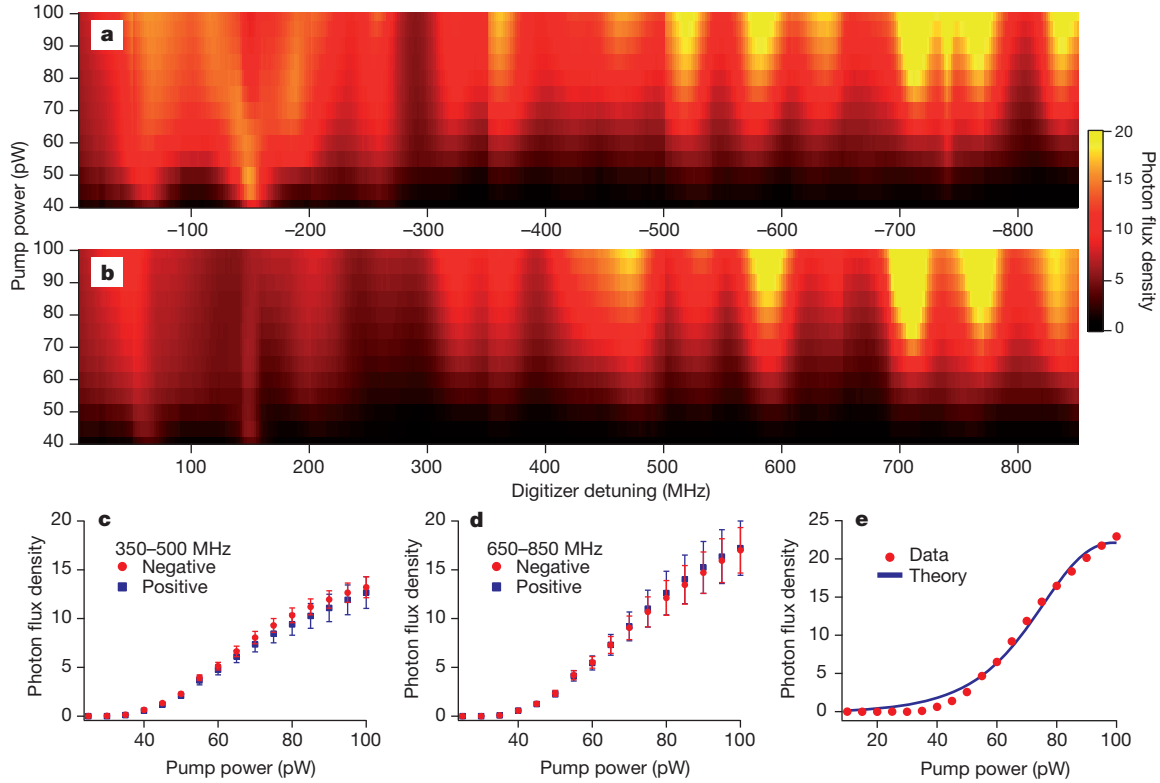

Figure 2 | Photons generated by the dynamical Casimir effect. Here we show the output flux of the transmission line while driving sample 1 at $f_d = 10.30$ GHz. **a**, **b**, Broadband photon generation. We plot the dimensionless photon flux density, n_{out} (photons s^{-1} Hz^{-1}), which is the measured power spectral density normalized to the photon energy, $\hbar\omega$, as a function of pump power and detuning, $\delta\omega/2\pi$. Panel **a** shows negative detunings (axis reversed), while **b** shows positive detunings. The symmetry of the spectrum is apparent. Positive and negative detunings are recorded simultaneously. The plots are stitched together from several separate scans, between which we have changed image rejection filters at the input of the analysers. **c**, **d**, The photon flux density for positive and negative detunings averaged over frequency (at fixed power) for two different symmetric bands, showing the symmetry of the spectrum. Error bars, s.d. **e**, A section through **a** at $\delta\omega/2\pi = -764$ MHz, along with a fit to the full theory of ref. 17.

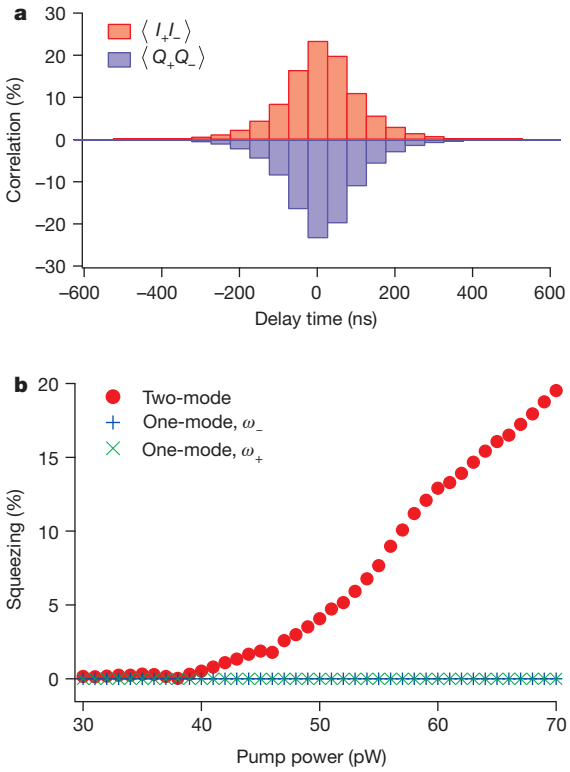

to the observable (Hermitian) quadrature operators $I_\pm$ and $Q_\pm$. We can write the TMS, σ_2, in terms of the quadratures as

$$\sigma_2 = \frac{1}{P_{avg}}\left(\langle I_+ I_- \rangle - \langle Q_+ Q_- \rangle\right) \quad (2)$$

where $P_{avg} = \left(\langle I_+^2 \rangle + \langle Q_+^2 \rangle + \langle I_-^2 \rangle + \langle Q_-^2 \rangle\right)/2$ is the average noise power in the sidebands and $\langle ... \rangle$ denotes the expectation value (Supplementary Information). We also expect a special structure for the correlations, in particular that $\langle I_+ I_- \rangle = -\langle Q_+ Q_- \rangle$ and that $\langle I_+ Q_- \rangle = \langle I_- Q_+ \rangle$. Finally, we comment[25] that by the proper choice of analysis phase, we can specify $\langle I_+ Q_- \rangle = \langle I_- Q_+ \rangle = 0$ without loss of generality, which has been done in writing equation (2) (see Supplementary Information and Supplementary Fig. 4).

To measure the correlations, we use a single amplifier but take advantage of the fact that the amplifier noise at different frequencies is uncorrelated. After amplifying, we split the signal into two separate analysis chains. We then calculate the four time-averaged IQ cross-correlation functions. Typical results are shown in Fig. 3. We see very clear cross-correlations that are ~1,000 times larger than the parasitic amplifier correlation (see Supplementary Fig. 3). Also, we see that

Figure 3 | Two-mode squeezing of the DCE field. **a**, The normalized cross-correlation functions $\langle I_+ I_- \rangle / P_{avg}$ and $\langle Q_+ Q_- \rangle / P_{avg}$, measured on sample 1, using $f_d = 10.30$ GHz and $|\delta\omega/2\pi| = 833$ MHz. We clearly see cross-correlations of the order of 25%, and that $\langle I_+ I_- \rangle = -\langle Q_+ Q_- \rangle$, as predicted. The shape of the correlation functions in delay time is determined by the filtering of the time traces. **b**, The two-mode squeezing, σ_2, of the field along with the one-mode squeezing, σ_1, at both ω_+ and ω_- as a function of drive power, measured on sample 1 at $|\delta\omega/2\pi| = 588$ MHz. We see that σ_2 clearly increases while the single-mode fields remain unsqueezed.

indeed $\langle I_+ I_- \rangle = -\langle Q_+ Q_- \rangle$, as we expect for TMS. The correlations imply a value of $\sigma_2 \approx 0.46$, which compares well to the predicted maximum squeezing of 50%.

Theory further predicts[25] that, even though the field is two-mode squeezed, if we look at either sideband frequency individually, it will remain unsqueezed, essentially appearing as a thermal field at some effective temperature. In Fig. 3b, we plot the TMS of the field, σ_2, along with the one-mode squeezing, $\sigma_1 = (\langle I^2 \rangle - \langle Q^2 \rangle)/(\langle I^2 \rangle + \langle Q^2 \rangle)$ at both frequencies, ω_+ and ω_-, as a function of drive power. We clearly see that σ_2 increases as a function of drive power while the one-mode fields remain unsqueezed.

In the Supplementary Discussion, we consider, and rule out, a number of spurious effects that could be the source of n_{out}. However, even if we assume that the photon creation is connected to the non-adiabatic modulation of the boundary condition, we need to confirm that it is seeded by vacuum fluctuations, not by spurious noise in the measurement system. To check this, we measured n_{out} with the cryostat temperature elevated to 250 mK, which is roughly $\hbar\omega_{\mathrm{d}}/2k_{\mathrm{B}}$. The direct comparison of the fluxes is complicated by the fact the aluminium CPW becomes lossy at this temperature, so some power will be lost. Still, we measure the ratio of the output fluxes to be 1.4 ± 0.3, which agrees with the expected value of 1.6 assuming the starting temperature is 50 mK. This tells us that $n_{\mathrm{in}} \ll 1$ at the base temperature, and that our system is therefore dominated by vacuum effects.

Received 31 August; accepted 15 September 2011.

1. Scully, M. O. & Zubairy, M. S. *Quantum Optics* (Cambridge Univ. Press, 1997).
2. Greiner, W. & Schramm, S. Resource letter QEDV-1: the QED vacuum. *Am. J. Phys.* **76,** 509–518 (2008).
3. Moore, G. Quantum theory of the electromagnetic field in a variable-length one-dimensional cavity. *J. Math. Phys.* **11,** 2679–2691 (1970).
4. Dodonov, V. Current status of the dynamical Casimir effect. *Phys. Scripta* **82,** 038105 (2010).
5. Dalvit, D. A. R., Neto, P. A. M. & Mazzitelli, F. D. Fluctuations, dissipation and the dynamical Casimir effect. Preprint at ⟨http://arXiv.org/abs/1006.4790v2⟩ (2010).
6. Casimir, H. B. G. On the attraction between two perfectly conducting plates. *Proc. K. Ned. Akad. Wet. B* **51,** 793 (1948).
7. Lamoreaux, S. K. Casimir forces: still surprising after 60 years. *Phys. Today* **60,** 40–45 (2007).
8. Braggio, C. *et al.* A novel experimental approach for the detection of the dynamical Casimir effect. *Europhys. Lett.* **70,** 754–760 (2005).
9. Yablonovitch, E. Accelerating reference frame for electromagnetic waves in a rapidly growing plasma: Unruh-Davies-Fulling-Dewitt radiation and the nonadiabatic Casimir effect. *Phys. Rev. Lett.* **62,** 1742–1745 (1989).
10. Lozovik, Y., Tsvetus, V. & Vinogradov, E. Femtosecond parametric excitation of electromagnetic field in a cavity. *JETP Lett.* **61,** 723–729 (1995).
11. Dodonov, V., Klimov, A. & Nikonov, D. Quantum phenomena in nonstationary media. *Phys. Rev. A* **47,** 4422–4429 (1993).
12. Schützhold, R., Plunien, G. & Soff, G. Quantum radiation in external background fields. *Phys. Rev. A* **58,** 1783–1793 (1998).
13. Kim, W., Brownell, J. & Onofrio, R. Detectability of dissipative motion in quantum vacuum via superradiance. *Phys. Rev. Lett.* **96,** 200402 (2006).
14. Liberato, S., Ciuti, C. & Carusotto, I. Quantum vacuum radiation spectra from a semiconductor microcavity with a time-modulated vacuum Rabi frequency. *Phys. Rev. Lett.* **98,** 103602 (2007).
15. Günter, G. *et al.* Sub-cycle switch-on of ultrastrong light–matter interaction. *Nature* **458,** 178–181 (2009).
16. Johansson, J. R., Johansson, G., Wilson, C. M. & Nori, F. Dynamical Casimir effect in a superconducting coplanar waveguide. *Phys. Rev. Lett.* **103,** 147003 (2009).
17. Johansson, J. R., Johansson, G., Wilson, C. M. & Nori, F. Dynamical Casimir effect in superconducting microwave circuits. *Phys. Rev. A* **82,** 052509 (2010).
18. Wilson, C. M. *et al.* Photon generation in an electromagnetic cavity with a time-dependent boundary. *Phys. Rev. Lett.* **105,** 233907 (2010).
19. Dezael, F. & Lambrecht, A. Analogue Casimir radiation using an optical parametric oscillator. *Europhys. Lett.* **89,** 14001 (2010).
20. Nation, P. D., Johansson, J. R., Blencowe, M. P. & Nori, F. Stimulating uncertainty: amplifying the quantum vacuum with superconducting circuits. *Rev. Mod. Phys.* (in the press); preprint at ⟨http://arXiv.org/abs/1103.0835v1⟩ (2011).
21. Sandberg, M. *et al.* Tuning the field in a microwave resonator faster than the photon lifetime. *Appl. Phys. Lett.* **92,** 203501 (2008).
22. Fulling, S. A. & Davies, P. C. W. Radiation from a moving mirror in two dimensional space-time: conformal anomaly. *Proc. R. Soc. Lond. A* **348,** 393–414 (1976).
23. Lambrecht, A., Jaekel, M. & Reynaud, S. Motion induced radiation from a vibrating cavity. *Phys. Rev. Lett.* **77,** 615–618 (1996).
24. Dodonov, V., Klimov, A. & Man'ko, V. Generation of squeezed states in a resonator with a moving wall. *Phys. Lett. A* **149,** 225–228 (1990).
25. Caves, C. M. & Schumaker, B. L. New formalism for 2-photon quantum optics. 1. Quadrature phases and squeezed states. *Phys. Rev. A* **31,** 3068–3092 (1985).
26. Yurke, B. & Denker, J. S. Quantum network theory. *Phys. Rev. A* **29,** 1419–1437 (1984).
27. Hoi, I.-C. *et al.* Demonstration of a single-photon router in the microwave regime. *Phys. Rev. Lett.* **107,** 073601 (2011).
28. Spietz, L., Lehnert, K., Siddiqi, I. & Schoelkopf, R. Primary electronic thermometry using the shot noise of a tunnel junction. *Science* **300,** 1929–1932 (2003).

Supplementary Information is linked to the online version of the paper at www.nature.com/nature.

Acknowledgements We thank G. Milburn and V. Shumeiko for discussions, and J. Aumentado and L. Spietz for providing the shot-noise thermometer. C.M.W., P.D., G.J., A.P. and M.S. were supported by the Swedish Research Council, the Wallenberg Foundation, STINT and the European Research Council. F.N. and J.R.J. acknowledge partial support from the LPS, NSA, ARO, DARPA, AFOSR, NSF grant no. 0726909, Grant-in-Aid for Scientific Research (S), MEXT Kakenhi on Quantum Cybernetics, and the JSPS-FIRST programme. T.D. acknowledges support from STINT and the Australian Research Council (grants DP0986932 and FT100100025).

Author Contributions The experimental work was carried out by C.M.W., A.P., M.S., T.D. and P.D. The theoretical work was performed by J.R.J., F.N., C.M.W. and G.J.

Author Information Reprints and permissions information is available at www.nature.com/reprints. The authors declare no competing financial interests. Readers are welcome to comment on the online version of this article at www.nature.com/nature. Correspondence and requests for materials should be addressed to C.M.W. (chris.wilson@chalmers.se).